

**OPEN ACCESS**

## Delamination-Debond Behaviour of Composite T-Joints in Wind Turbine Blades

To cite this article: H Gulasik and D Coker 2014 *J. Phys.: Conf. Ser.* **524** 012043

View the [article online](#) for updates and enhancements.

### You may also like

- [Analysis of Hollow Shape Semi Rigid Joints Made by Use of Thermal Drilling Technology](#)  
Pawel Bednarek and Jan Rzakowski
- [Laser welding process evaluation on stake-welded T-joints](#)  
Qinghua Lu, Zhishui Yu, Peilei Zhang et al.
- [Numerical study of nonlinear interaction of the guided wave due to breathing type debonding in stiffened panel](#)  
Abhijeet Kumar, Sauvik Banerjee and Anirban Guha



**ECS**  
The  
Electrochemical  
Society  
Advancing solid state &  
electrochemical science & technology

**DISCOVER**  
how sustainability  
intersects with  
electrochemistry & solid  
state science research

# Delamination-Debond Behaviour of Composite T-Joints in Wind Turbine Blades

H Gulasik<sup>3</sup>, D Coker<sup>1,2</sup>

<sup>1</sup> Assoc. Prof., Dept. of Aerospace Engineering, METU, 06800 Ankara, Turkey

<sup>2</sup> Assoc. Prof., METU Center for Wind Energy (METUWIND), 06800 Ankara, Turkey

<sup>3</sup> Ph.D. Student, Dept. of Aerospace Engineering, METU, 06800 Ankara, Turkey

E-mail: coker@metu.edu.tr

**Abstract.** Wind turbine industry utilizes composite materials in turbine blade structural designs because of their high strength/stiffness to weight ratio. T-joint is one of the design configurations of composite wind turbine blades. T-joints consist of a skin panel and a stiffener co-bonded or co-cured together with a filler material between them. T-joints are prone to delaminations between skin/stiffener plies and debonds between skin-stiffener-filler interfaces. In this study, delamination/debond behavior of a co-bonded composite T-joint is investigated under 0° pull load condition by 2D finite element method. Using Abaqus<sup>®</sup> commercial FE software, zero-thickness cohesive elements are used to simulate delamination/debond in ply interfaces and bonding lines. Pulling load at 0° is applied and load-displacement behavior and failure scenario are observed. The failure sequence consists of debonding of filler/stringer interface during one load drop followed by a second drop in which the 2<sup>nd</sup> filler/stringer debonds, filler/skin debonding and skin delamination leading to total loss of load carrying capacity. This type of failure initiation has been observed widely in the literature. When the debond strength is increased 30%, failure pattern is found to change in addition to increasing the load capacity by 200% before total loss of loading carrying capacity occurs. Failure initiation and propagation behavior, initial and max failure loads and stress fields are affected by the property change. In all cases mixed-mode crack tip loading is observed in the failure initiation and propagation stages. In this paper, the detailed delamination/debonding history in T-joints is predicted with cohesive elements for the first time.

Keywords: Composite wind turbine blade, T-joint (T-section), Delamination/Debond, Cohesive Zone Method (CZM)

## 1. Introduction

Wind turbine blades, composed of skin panels and stiffeners, are manufactured by using laminated composite materials. They are mainly used for their high strength/stiffness to weight ratio. Some other advantageous characteristics of composites are: manufacturing abilities, corrosion resistance etc. [5, 12, 13]. Therefore, there is an increasing demand for composite materials in wind turbine, aerospace, marine and automobile industries.

Despite their advantages, laminated composites have also some weak points. They are dominated by matrix properties in through thickness direction and in general, there is no other strengthening mechanism. This situation makes them relatively weak in through thickness direction. Therefore, plies



separate from each other under loading which is known as delamination. Another failure mechanism similar to the delamination in composite structures is the debonding of the parts from each other whereas delamination is the separation of individual plies in the part. Mechanisms driving debonding are also similar to delamination mechanisms. Therefore, debond can be treated as delamination in numerical simulations. Some material, design and manufacturing aspects are considered to be critical for delamination/debond: skin-stiffener section, curved laminates, ply drop-off, manufacturing defects, drilling, etc. [3, 11, 14]. Under various loading conditions (mechanical, buckling, cyclic, hydrothermal, low velocity impact, bird strike, underwater explosion, lightning, etc. [2, 3, 4, 5, 14, 21]), interlaminar normal and shear stresses are generated between the composite plies in these critical regions which cause delaminations/debonds. Delamination/debond reduces the stiffness and strength of the structure as the delaminated area gets larger. Structural integrity of the structure is lost and a sudden collapse of the structure is observed at a critical level of the delaminated area.

T-joint (T-section, tee joint), as an example of composite wind turbine cross-section, is prone to delamination/debond failure. T-joints are composed of a skin panel and stiffeners, co-cured or co-bonded together with a filler between them as seen in Figure 1. In T-joints, because of the stiffness difference between the skin and the stiffeners, a complex 3D stress state is generated in the structure. This makes the T-joint a critical delamination/debond region. Delaminations can be seen between the skin panel or stiffener plies, debonds can be seen between the skin-stiffener-filler interfaces. Generally, the delamination/debond process results in a sudden collapse of the T-joint.

The aim of this manuscript is to study the competing mechanisms of delamination/debond failure of a composite T-joint and the change of failure process (delamination vs debond) with bond strength using finite element analysis with cohesive zone model in 2D. Quasi-static  $0^\circ$  pull load loads are applied and the load-displacement curves, failure initiation and propagation scenarios are investigated.

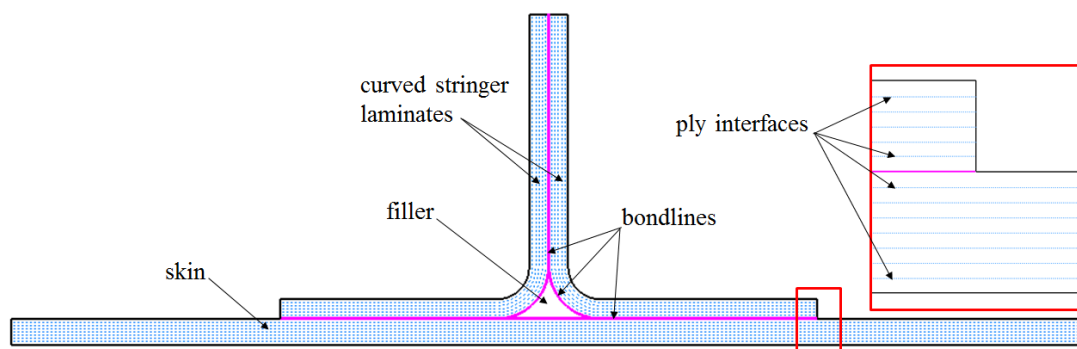


**Figure 1-** Geometry of a typical T-joint

## 2. Cohesive Zone Method (CZM)

Laminated composite materials are composed of plies which are connected to each other with almost zero thickness matrix or adhesive materials. CZM is used to simulate delamination/debond between these ply interfaces. In CZM, there is no need to place an initial crack manually in the numerical model. Cracks can initiate in cohesive layers anywhere in the structure which allows multiple crack initiations and propagations as an outcome of the model. Because of these advantageous characteristics, CZM is being increasingly used in delamination/debond modeling in laminated composites.

A cohesive element can be considered as two separate faces. Initially, these faces are in contact and the element is at the zero stress state. As the load is applied, element faces separate from each other in Mode I and Mode II fracture directions for a 2D case. Cohesive layer is then assumed to be damaged according to a considered cohesive law which relates interface tractions to interface displacements. Some of the generally used cohesive laws are bilinear [7, 8, 18], exponential [15] and trapezoidal [16,

17] laws which are shown in Figure 2, where,  $t_i^0$  is the interfacial strength and  $\delta_i^0$  is the interfacial displacement for damage initiation,  $\delta_i^c$  is the critical displacement for crack growth and  $\delta_i^s$  is the softening displacement for trapezoidal law;  $i=I, II, III$  stands for fracture modes I, II and III. Bilinear cohesive law is used in this study.

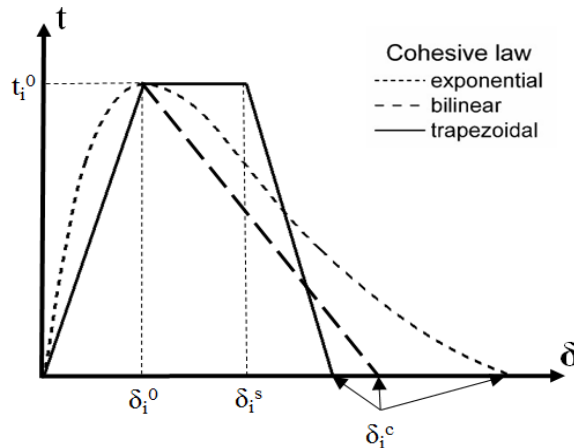


**Figure 2-** Exponential, bilinear and trapezoidal cohesive laws

### 2.1. Single Mode Delamination

The constitutive behavior of a cohesive element for a single fracture mode with bilinear cohesive law can be defined as [7, 9]:

$$\left. \begin{array}{ll} k_i^0 \delta_i & \delta_i \leq \delta_i^0 \\ (1-d)k_i^0 \delta_i & \delta_i^0 < \delta_i < \delta_i^c \\ 0 & \delta_i \geq \delta_i^c \end{array} \right\} = t_i \quad (1)$$

where  $\delta_i$  is the displacement at an arbitrary point and  $k_i^0$  is the penalty stiffness.

Damage of the cohesive elements is assumed to start after damage initiation displacement  $\delta_i^0$  or damage initiation traction  $t_i^0$ . Up to damage initiation point, material behavior is assumed to be linear with penalty stiffness. In numerical applications, the penalty stiffness is chosen to be high enough to maintain the correct load transfer between the layers and prevent the interpenetration of the interface and low enough to get rid of numerical instabilities. After damage initiation, a scalar damage parameter,  $d$ , is used to track the damage evolution in the loading history. The damage variable varies from 0 at the initial damage point to 1 at the critical displacement. The area under traction-separation curve is the critical energy release rate (fracture toughness)  $G_{ic}$  of the material and can be calculated as:

$$G_{ic} = \frac{t_i^0 \delta_i^c}{2} = \frac{k_i^0 \delta_i^0 \delta_i^c}{2} \quad (2)$$

After the fracture toughness,  $G_{ic}$ , or the critical displacement,  $\delta_i^c$ , is achieved, cohesive element does not carry further load and crack growth initiates.

### 2.2. Mixed-Mode Delamination

Delamination in composite materials is generally a combination of Mode I, Mode II and Mode III. In single mode delamination, initiation is satisfied with allowable tractions ( $t_i^0$ ) or displacements ( $\delta_i^0$ ) of the interface. For the mixed-mode, delaminations can take place before any single mode allowable. Therefore, interactions of tractions or displacements are used in mixed-mode conditions for

delamination initiation. A generally used mixed-mode initiation criterion is the quadratic power law interaction of single mode tractions:

$$\left(\frac{\langle t_I \rangle}{t_I^0}\right)^2 + \left(\frac{t_{II}}{t_{II}^0}\right)^2 + \left(\frac{t_{III}}{t_{III}^0}\right)^2 \geq 1 \quad (3)$$

where,  $t_I, t_{II}, t_{III}$  are the traction components at an arbitrary point.

Similar to delamination initiation, interaction equations are used to determine delamination propagation in mixed-mode. Benzeggagh-Kenane (BK) Law [7, 9, 20, 22] is one of the most used mixed-mode propagation laws and is given as:

$$G_C \geq G_{IC} + (G_{IIC} - G_{IC}) \left(\frac{G_{II}}{G_I + G_{II}}\right)^\eta \quad (4)$$

where  $\eta$  is the BK law exponent extracted from experimental results by curve fitting.

### 3. T-joint Study

#### 3.1. Critical Regions in T-joints for Delamination/Debond

Delamination/debond failure is caused by the interlaminar normal and shear stresses between different constituents of the structure. Failure mechanism and exact location may differ depending on the design parameters; radius, thickness, layup, filler stiffness, etc. The literature survey of T-joints shows that filler region and flange tips are the critical locations for delamination/debond initiation. Two of the major initiation mechanisms observed in the literature are the debond of the filler/stringer interface [10, 19, 23] as shown in Figure 3 and the delamination of plies in the stringer laminate at the curved region [1, 3, 4, 6] as shown in Figure 4.

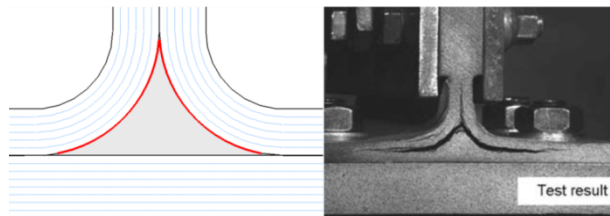


**Figure 3-** Debond between filler/stringer interfaces [19]

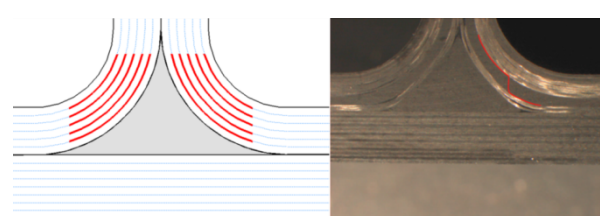


**Figure 4-** Delamination between stringer plies [6]

#### 3.2. T-joint Geometry and the Finite Element Model

A T-joint can be divided into four main parts: 1) left stringer leg, 2) right stringer leg, 3) skin and 4) filler, where four parts are connected to each other with bonding lines as shown in Figure 5. Figure 5 and Table 1 present the detailed geometry of the T-joint where “ $t_{ply}$ ”, “ $t_{st}$ ”, “ $t_s$ ” are the thicknesses of the single ply, stringer and skin, respectively, “ $L_{st}$ ” and “ $L_s$ ” are the length of the stringer and the skin, respectively, “ $h_{st}$ ” is the height of the stringer.

IM7/8552 composite material elastic and interface properties for skin and stringer legs and FM300 adhesive material elastic and interface properties for filler and bonding lines are used which are presented in Table 2 and Table 3 [2, 24].  $0^\circ$  ply direction is defined to be in the direction of the stringer, namely out of plane direction in this case. Auxiliary coordinate frames are assigned for composite and filler materials to describe the material and stress component directions as seen in Figure 6.

An FE model is constructed with Abaqus in 2D with plane strain assumption as shown in Figure 6. The stringer legs and the skin are modeled with CPE4I (2D, plane strain, quadrilateral, 4 node, incompatible mode) elements with anisotropic properties whereas the filler is modeled as an isotropic material with CPE4I/CPE3 elements. Cohesive layers are modeled with COH2D4 (2D, cohesive, 4

node) elements between each layer of the stringer and the skin laminates and bonding lines. In total, there are 19260 CPE4I, 7 CPE3, 8669 COH2D4 elements and 28906 nodes in the FE model. In numerical simulations, a viscosity parameter, with a value of  $1e-5$ , is used for cohesive elements to ease the numerical convergence which gives a small viscous dissipation energy compared to the total energy of the structure. The quadratic stress interaction for delamination initiation and BK criterion for delamination propagation are used. The skin panel is clamped at both ends and prescribed displacement is applied at the top edge of the stringer in the vertical direction in a quasi-static manner and implicit non-linear solutions with line search method are carried out [9].

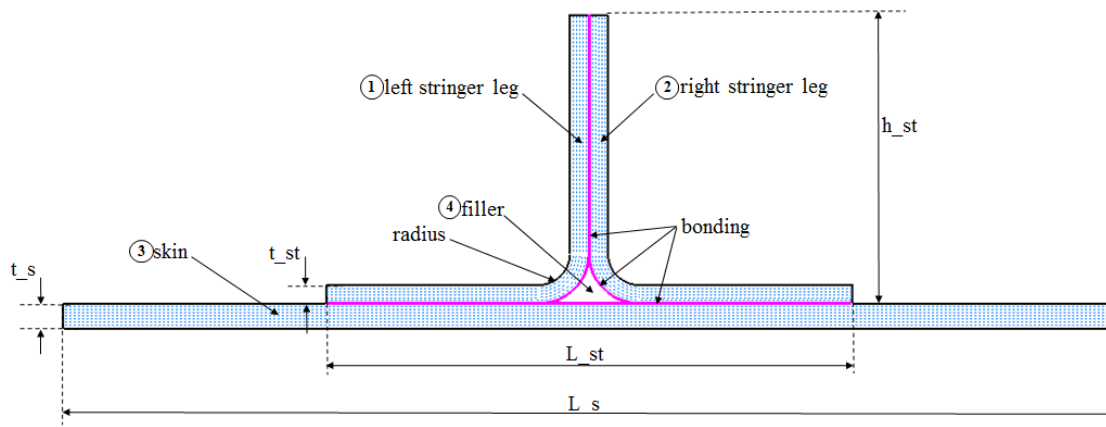


Figure 5- T-joint geometry and dimensions

Table 1– T-joint dimensions and lay-up [2]

t_ply [mm]	h_st [mm]	t_st [mm]	L_st [mm]	radius [mm]	t_s [mm]	L_s [mm]	stiffener layup	skin layup
0.15	28.0	0.90	56.0	3.0	1.20	156.0	[45 <sub>2</sub> /0 <sub>2</sub> /90 <sub>2</sub> ]	[45 <sub>2</sub> /0/90] <sub>s</sub>

Table 2– Elastic properties of the IM7/8552 composite and FM300 adhesive materials

	E11 [GPa]	E22 [GPa]	E33 [GPa]	G12 [GPa]	G13 [GPa]	G23 [GPa]	v12	v13	v23
IM7/8552	147	11.8	11.8	6.0	6.0	4.0	0.30	0.30	0.475
FM300 (isotropic)	2.38	-	-	0.68	-	-	-	-	-

Table 3– Interface properties of the IM7/8552 composite and FM300 adhesive materials

	k <sub>I</sub> <sup>0</sup> [MPa/mm]	k <sub>II</sub> <sup>0</sup> [MPa/mm]	k <sub>III</sub> <sup>0</sup> [MPa/mm]	t <sub>I</sub> <sup>0</sup> [MPa]	t <sub>II</sub> <sup>0</sup> [MPa]	t <sub>III</sub> <sup>0</sup> [MPa]	G <sub>IC</sub> [N/mm]	G <sub>IIC</sub> [N/mm]	G <sub>IIIC</sub> [N/mm]	η
IM7/8552	1e6	1e6	1e6	50	100	100	0.9	2.5	2.5	8
FM300	1e6	1e6	1e6	60	90	90	0.243	0.514	0.514	4.6

### 3.3. Numerical Results

Numerical investigations of the T-joint for 0° pull load are conducted in three sections:

- In the first section, two FE models with and without cohesive layers are compared.
- In the second section, the load-displacement curve, stress fields and delamination/debond behavior of the T-joint with cohesive layers are investigated in detail.

- In the third section, second delamination/debond initiation mechanism mentioned in Section 3.1 is captured by increasing the interface strength of the adhesive material.

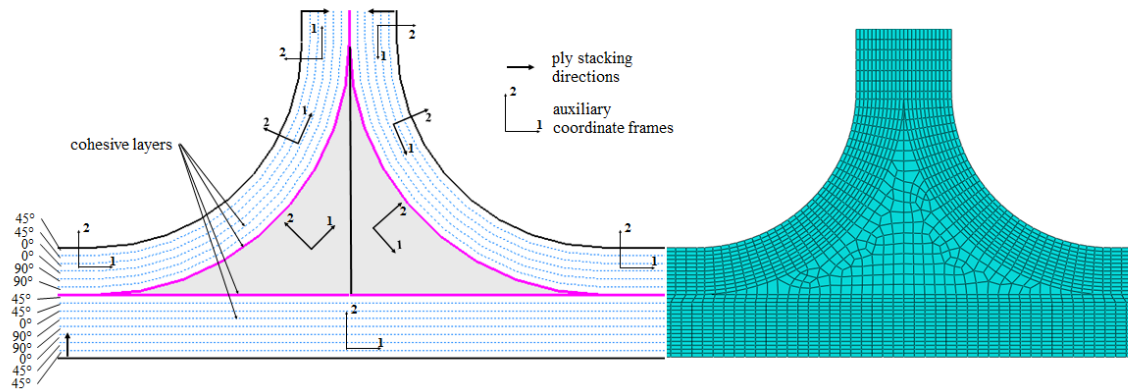


**Figure 6-** Finite element model of the T-joint.

**3.3.1. Cohesive vs Non-Cohesive Model:** The load–displacement curves for models with and without cohesive layers are shown in Figure 7 for 0° pull load. The solid line, with cohesive layers, follows the non-cohesive model curve until the initial failure at a displacement of 6.91 mm. It can be seen that the stiffness of the two models are almost the same until the crack initiates. A slight difference in the load–displacement curve is observed which is caused by the damage accumulation in the cohesive elements. The S22 and S12 stress fields for both models before failure (at pt1 in Figure 7) are almost identical for the two models (1st and 2nd stress component directions are shown in Figure 6). The good agreement of the load–displacement curve and the stress contours before the failure initiation shows that the multiple cohesive layers are successfully implemented and do not affect the elastic behavior.

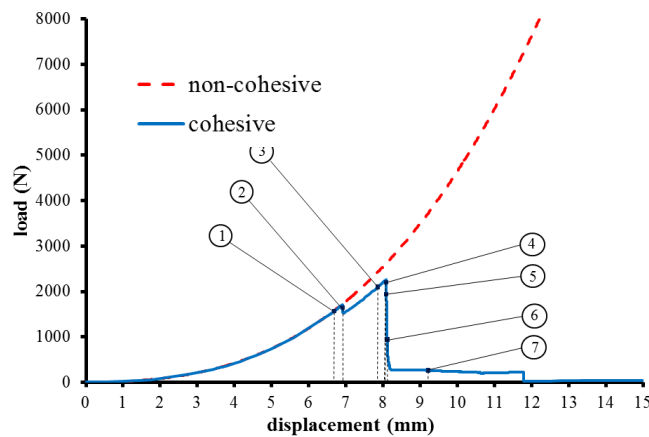


**Figure 7-** Load –displacement curves for non-cohesive and cohesive models for 0° pull load

**3.3.2. Delamination/debond process for cohesive model:** S22 and S12 stress contour plots for the cohesive model in the previous section during the delamination/debond initiation and the propagation processes are shown in Figure 8 (a-e), at points 1, 2, 3, 4 and 5 (Figure 7), respectively.

As seen in Figure 8 (a), filler corners are the high stress locations for S22 component and filler/stringer interface at the radius are the high stress locations for S12 component at pt1 (displacement = 6.60 mm, load=1517N) which is close to the initial debond displacement. Debond initiates at 78° from the horizontal axis as explained in the next paragraph. At the debond location, S22 is around 45 MPa and S12 is around 45 MPa which shows the mixed-mode delamination initiation.

Figure 8 (b) shows the stress contours at pt2 (6.91 mm displacement and 1675 N load). At the filler/right stringer interface in the curved region, an initial debond initiates with a length of 0.2 mm

(one element size) at  $78^\circ$  from the horizontal axis and propagates unstably where the crack tips are shown by the arrows in Figure 8 (b). A small load drop is seen with the initial debond as shown in Figure 7 and new stress fields are developed. Stress concentrations are developed at the crack tips. At the upper crack front, S22 is around 80 MPa and S12 is around 10 MPa indicating a Mode I dominated crack growth. At the lower crack front S22 is around 60 MPa and S12 is around 80 MPa indicating a mixed-mode crack growth.

Figure 8 (c) shows the stress contours at pt3 (7.86 mm displacement and 2101 N load) where debond has propagated in the lower and upper directions in the bonding line. Upper crack front grows through the stringer/stringer interface to some displacement from the filler tip and stabilizes, because left stringer starts to act as main load carrying member and load on the right stringer is eliminated. Lower crack stops at the filler corner because of the compressive S22 stress component. Therefore, the stable behaviour of the crack tips lead to an increase in the load-displacement curve from the local minimum of 1519 N with a decreased stiffness. Meantime, stress concentration at the filler/left stringer interface is still present. S22 stress component is around 50 MPa at the filler/left stringer interface at  $62^\circ$  from the horizontal axis and S12 component is around 45 MPa at the filler/left stringer interface at the  $22^\circ$  from the horizontal axis.

Figure 8 (d) shows the stress contours at pt4 (8.08 mm displacement and 2233 N load), near the maximum load point of 2256 N at the end of the stable crack growth, just before the next load drop. At pt4, a second debond initiates at the filler/left stringer at  $67^\circ$  from the horizontal axis. A sudden load drop is seen after the debond initiates. As in the right debond, the upper crack grows under Mode I dominated loading (S22=100 MPa, S12=10 MPa) and lower crack grows under mixed-mode loading (S22=80 MPa, S12=70 MPa).

Figure 8 (e) shows the stress contours at pt5 (8.08 mm displacement and 2127 N load). After the initiation, debond at the filler/left stringer interface rapidly grows in upper and lower directions and filler completely separates from the stringer. Stress concentrations are seen at the front of the rapidly growing crack tips. Until the separation of the filler from the stringers, the lower crack tip at the filler/right stringer interface does not propagate.

During debond/delaminations which occur in a single load drop, unstable crack growth leads to skin/stiffener debonding and delamination between skin plies as seen in Figures 9 (a) and (b) at pts6 and 7. Final failure of the structure occurs with the complete separation of stringers from the skin.

From the above discussion, it can be stated that filler area is critical in terms of delamination/debond initiation and propagation. Stress concentrations around this region cause initial cracks. Delamination/debond initiation and propagation show mixed-mode behaviour. High stress concentrations at the crack tips cause further crack propagation. Filler/stringer separation causes a significant load drop which shows the importance of the filler for structural integrity. T-joint almost fails during the sudden load drop. At the later stages of the process, delaminations are seen between the upper skin plies which stabilize the cracks and cause a residual strength. This shows the importance of modeling cohesive layers for the complete interface length.

**3.3.3. Failure Modes for  $0^\circ$  Pull Load:** The first delamination/debond initiation mechanism of the T-joints is the debond of the filler/stringer interfaces as shown in Figure 3. The considered T-joint in Section 3.3.2 also shows the first failure mechanism. The second failure mechanism is the delamination of the stringer plies as shown in Figure 4. In order to change the failure mechanism, the interface strength values ( $t_I^0$  and  $t_{II}^0$ ) of the FM300 adhesive material for Modes I and II are increased to 130% of its previous value.

Load-displacement curves for the base model and the increased interface strength are shown in Figure 5.10. For the increased strength, the area under the load-displacement curve, failure initiation load and maximum load increase in considerable amounts. There are four load drops on the curve indicating the gradual failure of the structure. First load drop point is at 2241 N, second load drop is at 3034 N, third load drop is at 4085 N and last drop is at 5504 N which is the maximum load point. Sudden load drop after the maximum load causes convergence problems, therefore load-displacement

and failure propagation cannot be captured for further displacement. The critical points (pt1 – pt6) are shown on the load-displacement curve of the increased strength which will be used to discuss the delamination/debond initiation and propagation process in detail.

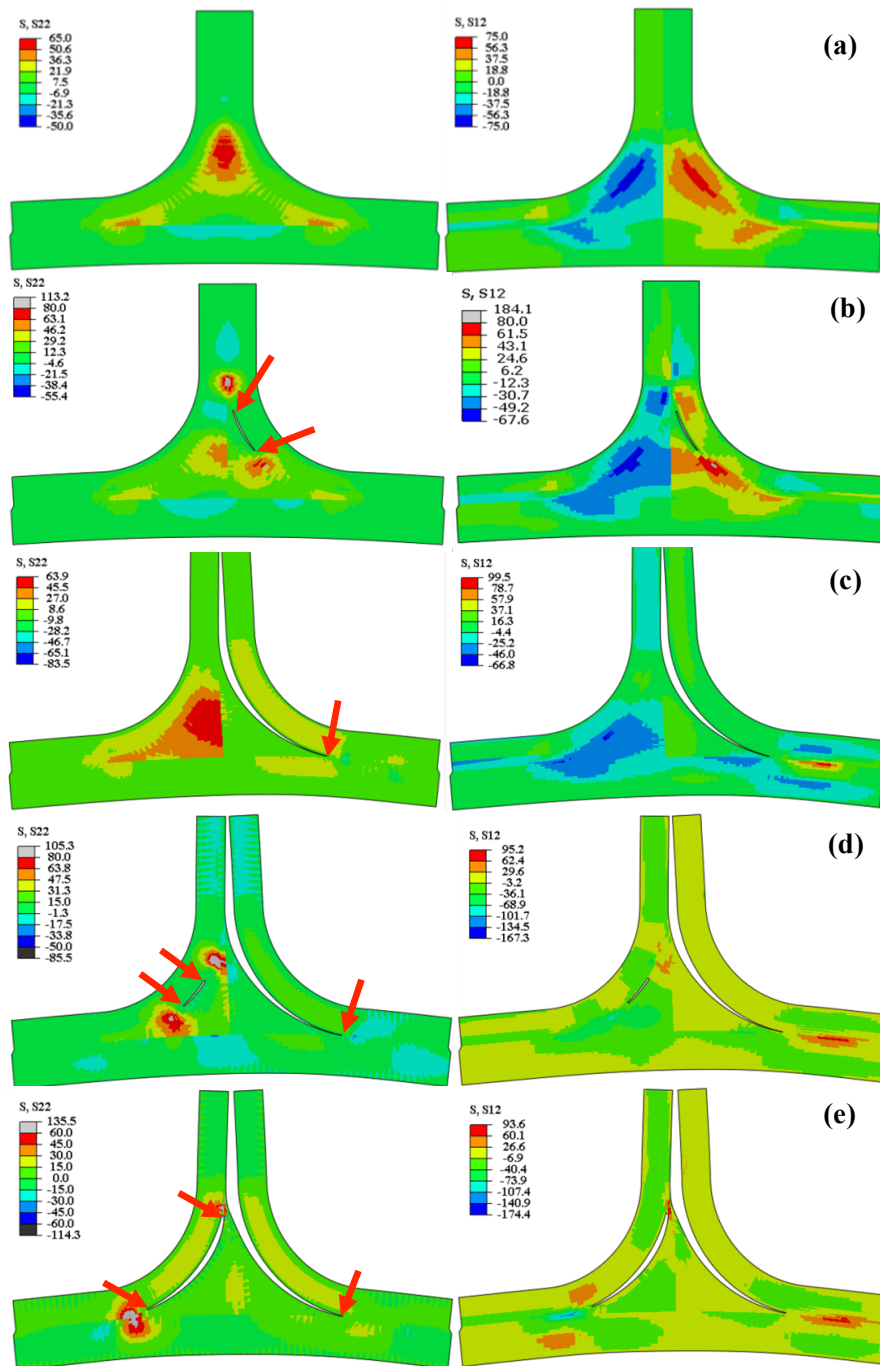


**Figure 8-**  $S_{22}$ [MPa] and  $S_{12}$ [MPa] stress components captured at critical points on the load-displacement curve of the cohesive model a) pt1 (displacement = 6.60 mm, load=1517N) b) pt2 (displacement = 6.91 mm, load=1675 N), c) pt3 (displacement = 7.86 mm, load=2101 N) , d) pt4 (displacement = 8.08 mm, load=2233 N), e) pt5 (displacement = 8.08 mm, load= 2127 N)

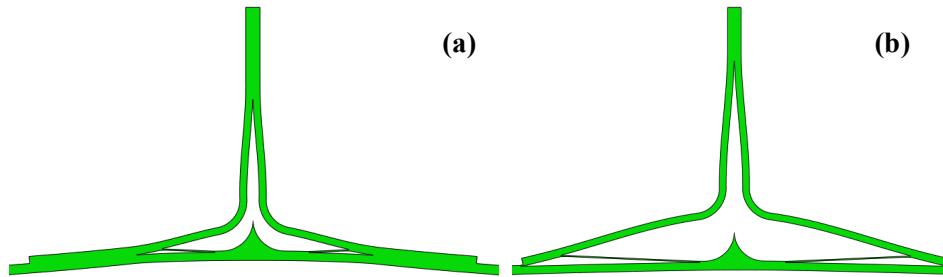


**Figure 9-** Delamination/debond propagation for the cohesive model a) pt6 (displacement = 8.11 mm, load=796 N), b) pt7 (displacement = 9.11 mm, load=262 N)

Delamination initiation/propagation scenario for the increased strength is shown in Figure 5.11 through the points 1, 2, 3, 4, 5 and 6 (Figure 5.10). Figures 5.11 (a) correspond to the initial delamination point. An initial delamination with 0.60 mm length (3 element size) is seen between 5th and 6th right stringer plies (at pt1 with 7.65 mm displacement and 2234 N load) at 72° from the horizontal axis. The initial delamination causes a small load drop on the load-displacement curve as seen in Figure 5.10. After the initial failure, delamination grows in upper and lower directions suddenly. With the increasing displacement, upper crack front slows after 3.53 mm above the upper filler corner and lower crack front slows after 5.13 mm from the right filler corner. Therefore, load starts to increase after the initial drop. With the increase in displacement, another delamination is seen between 5th and 6th left stringer plies (at pt2 with 8.78 mm displacement and 3030 N load) as seen in Figure 5.11 (b). This delamination causes a load drop on the load-displacement curve. After the initial sudden growth, upper crack stops 2.54 mm above the upper filler corner and lower crack front slows after 6.52 mm from the left filler corner. Therefore, load starts to increase with the increase in displacement once again. A debond is seen in at the filler/right stringer interface (at pt3 with 10.01 mm displacement and 4077 N load) and a delamination is seen between the skin upper plies near the right filler corner as seen in Figure 5.11 (c). After the last delamination and debond, all the crack fronts stabilizes and load starts to increase until the maximum load point (11.51 mm displacement and 5504 N load). Near the maximum load point, a debond at the filler/left stringer interface (at pt4 with 11.51 mm displacement and 5493 N load) and a delamination between the upper skin plies near to the right filler corner (at pt5 with 11.51 mm displacement and 5396 N load) appear as shown in Figure 5.11 (d) and (e). Excessive delamination/debonds (at pt6 with 11.52 mm displacement and 4697 N load) are shown in Figure 5.11 (f) at the last step of the sudden load drop. Sudden load drop causes convergence problems, therefore failure propagation cannot be captured further.

In summary, the area under the load-displacement curve, initial failure load and displacement, maximum failure load and displacement are increased by considerable amounts for the increased interface strength values of the adhesive material compared to the base model. A 30% increase in interface strength results in more than 200% increase in maximum failure load. Failure initiation and propagation scenario is also changed. Delamination between the stringer plies are observed in addition to debonds at the filler/stringer interfaces and delaminations between the skin plies.

#### 4. Conclusion

In this study, delamination/debond behavior of a co-bonded composite T-joint is investigated under 0° pull load by 2D finite element method. Using Abaqus® commercial FE software, zero-thickness cohesive elements are used to simulate delamination/debond in ply interfaces and bonding lines.

Load-displacement behavior and failure scenario of the T-joint are observed for 0° pull load. It is seen that a debond starts at the filler/stringer interface at the curved region. Delamination/debond initiates and propagates in mixed-mode. Delamination/debond initiation during the loading corresponds to the load drops on the load-displacement curve. Sudden collapse of the structure is seen with sudden increase in delamination/debond region.

A different failure initiation mechanism of the T-joint is observed by changing the interface strength of the adhesive material for 0° pull load. Failure initiation and propagation behaviors, load displacement curve, initial and max failure loads and stress fields are affected by the property changes.

By modeling multiple cohesive layers in the structure, multiple delaminations/debonds during the complete loading history are captured. Additionally, the residual strength of the T-joints and multiple load drops on the load-displacement curves are captured.

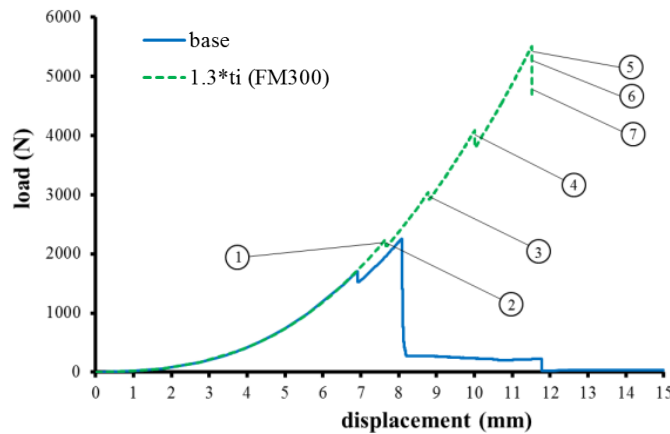


**Figure 5.10-** Load–displacement curves for the base material and the increased interface strength material under 0° pull load.

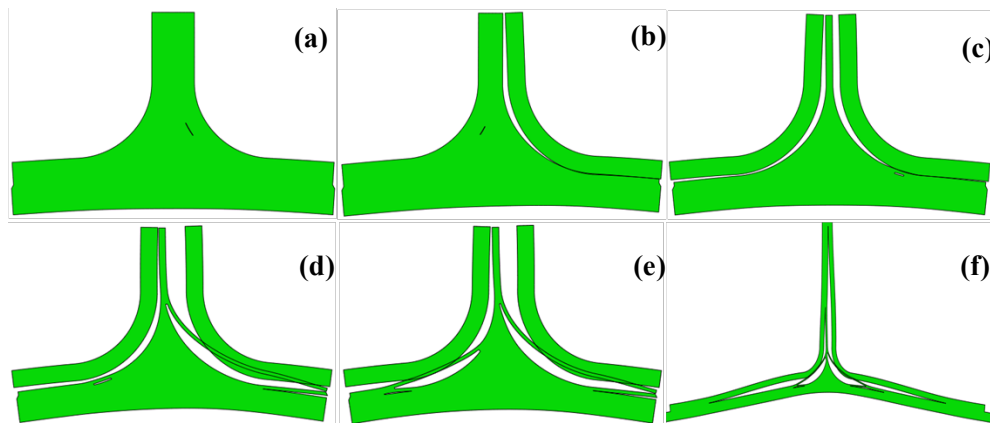


**Figure 5.11-** Delamination/debond propagation for the increased interface strength of the FM300 adhesive material a) pt1 (displacement = 7.65 mm, load = 2234 N), b) pt2 (displacement = 8.78 mm, load = 3030 N), c) pt3 (displacement = 10.01 mm, load = 4077 N), d) pt4 (displacement = 11.51 mm, load = 5493 N), e) pt5 (displacement = 11.51 mm, load = 5396 N), f) pt6 (displacement = 11.52 mm, load = 4697 N).

## References

- [1] Orifici, A.C., Shah, S.A., Herszberg, I., Kotler, A., Weller, T., “Failure Analysis in Postbuckled Composite T-Sections”, *Composite Structures* 86 (2008) 146–153.
- [2] Orifici, A.C., Thomson, R.S., Degenhardt, R., Bisagni, C., Bayandor, J., “A Finite Element Methodology for Analyzing Degradation and Collapse in Postbuckling Composite Aerospace Structures”, *Journal of Composite Materials*, Vol. 0, No. 00/2009.
- [3] Mandell, J.F., Cairns, D.S., Samborsky, D.D., Morehead, R.B., Haugen D.J., “Prediction of Delamination in Wind Turbine Blade Structural Details”, *Journal of Solar Energy Engineering-transactions of The Asme - J SOL ENERGY ENG* 01/2003; 125(4).
- [4] Phillips, H. J., Shenoi R.A., “Damage Tolerance of Laminated Tee Joints in FRP Structures”, *Composites Part A* 29A (1998) 465-478 1998.

- [5] Dharmawan, F., Thomson, R.S., Li, H., Herszberg, I., Gellert, E., “Geometry and Damage Effects in A Composite Marine T-Joint”, *Composite Structures* 66 (2004) 181–187.
- [6] Hélénon, F., Wisnom, M.R., Hallett, S.R., Trask R.S., “Numerical Investigation into Failure of Laminated Composite T-Piece Specimens Under Tensile Loading”, *Composites: Part A* 43 (2012) 1017–1027.
- [7] Camanho, P.P., Dávila, C.G., “Mixed-Mode Decohesion Finite Elements for the Simulation of Delamination in Composite Materials”, NASA/TM-2002-211737
- [8] Song, K., Dávila, C.G., Rose, C.A., “Guidelines and Parameter Selection for the Simulation of Progressive Delamination”, *Abaqus Users’ Conference*, 2008
- [9] *Abaqus/CAE V6.12 User's Manual*
- [10] Bruyneel, M., Delsemme, J.P., Jetteur, Ph., Germain, F., “Modeling Inter-Laminar Failure in Composite Structures: Illustration on an Industrial Case Study”, *Appl. Compos. Mater.* (2009) 16:149–162
- [11] Raju, I.S., O’Brien, T.K., “Fracture Mechanics Concepts, Stress Fields, Strain Energy Release Rates, Delamination Initiation and Growth Criteria”, Edited by Srinivasan Sridharan, *Delamination Behaviour Of Composites*, Woodhead Publishing, 2008
- [12] Tomblin, J., “Overview of Composite Material Trends in Aviation Manufacturing”, 2006, National Institute for Aviation Research (NIAR), Wichita State University, [http://webfiles.wichita.edu/cedbr/WIRED\\_comp\\_ov\\_5\\_14\\_08.pdf](http://webfiles.wichita.edu/cedbr/WIRED_comp_ov_5_14_08.pdf) (07 August 2013)
- [13] [http://www.boeing.com/commercial/aeromagazine/articles/qtr\\_4\\_06/article\\_04\\_1.html](http://www.boeing.com/commercial/aeromagazine/articles/qtr_4_06/article_04_1.html), (05 July 2013)
- [14] Riccio, A., “Delamination in the Context of Composite Structural Design”, Edited by Srinivasan Sridharan, *Delamination Behaviour of Composites*, Woodhead Publishing, 2008
- [15] Alfano, M., Furgiuele, F., Leonardi, A., Maletta, C., Paulino, G.H., “Fracture Analysis of Adhesive Joints Using Intrinsic Cohesive Zone Models”, *Atti del Congresso IGF19 Milano*, 2007.
- [16] Chowdhury, S.R., Narasimhan, R., “A Cohesive Finite Element Formulation For Modeling Fracture And Delamination In Solids”, *Sādhanā*, Vol. 25, Part 6, Dec 2000, pp. 561–587.
- [17] Tvergaard, V., Hutchinson, J.W., “The Relation Between Crack Growth Resistance And Fracture Process Parameters In Elastic-Plastic Solids”, *J. Mech. Phys. Solids* Vol. 40, No. 6, pp. 1377-1397, 1992.
- [18] Alfano, G., Crisfield, M. A., “Finite Element Interface Models For The Delamination Analysis Of Laminated Composites: Mechanical And Computational Issues”, *Int. J. Numer. Meth. Engng* 2001; 50:1701-1736 .
- [19] Davies, G.A.O., Ankensen, J., “Virtual Testing Of Realistic Aerospace Composite Structures”, *J Mater Sci* (2008) 43:6586–6592.
- [20] Camanho, P.P., Dávila, C.G., De Moura, M. F., “Numerical Simulation of Mixed-mode Progressive Delamination in Composite Materials”, *Journal of Composite Materials*, Vol. 37, No. 16, 2003.
- [21] Rao, V.V.S., Veni, K.K., Sinha, P.K., “Behavior of Composite wing T-joints in Hydrothermal Environments”, *Aircraft Engineering and Aerospace Technology*, Volume 76, Number 4, 2004, pp. 404–413.
- [22] Benzeggagh, M.L., Kenane, M., “Measurement Of Mixed-Mode Delamination Fracture Toughness Of Unidirectional Glass/Epoxy Composites With Mixed-Mode Bending Apparatus”, *Composites Science and Technology* 56 (1996) 439-449.
- [23] Chen, J., Fox, D., “Numerical investigation into multi-delamination failure of composite T-piece specimens under mixed mode loading using a modified cohesive model”, *Composite Structures* 94 (2012), 2010–2016.
- [24] Psarras, S., Pinho, S.T., Falzon, B.G., “Damage-Tolerant Design of Stiffener Run-Outs: A Finite Element Approach”, *InTech*, 2012.